Available online at www.sciencedirect.com
SCIENCE DIRECT®
Biomaterials 26 (2005) 3363–3376
Biomaterials
www.elsevier.com/locate/biomaterials

Age-related transparent root dentin: mineral concentration, crystallite size, and mechanical properties

J.H. Kinney[a,*], R.K. Nalla[b], J.A. Pople[c], T.M. Breunig[d], R.O. Ritchie[b]

[a]*Department of Mechanical Engineering and UCSF/UCB Joint Graduate Group in Bioengineering, Lawrence Livermore National Laboratory, 7000 East Ave., L-333, PO 808, Livermore, CA 94550, USA*
[b]*Materials Sciences Division, Lawrence Berkeley National Laboratory, and Department of Materials Science and Engineering, University of California, Berkeley, CA 94720, USA*
[c]*Stanford Synchrotron Radiation Laboratory, Stanford Linear Accelerator Center, Menlo Park, CA 94025, USA*
[d]*Coating Place, Inc., Verona, WI 53593, USA*

Received 3 June 2004; accepted 3 September 2004

Abstract

Many fractures occur in teeth that have been altered, for example restored or endodontically repaired. It is therefore essential to evaluate the structure and mechanical properties of these altered dentins. One such altered form of dentin is transparent (sometimes called sclerotic) dentin, which forms gradually with aging. The present study focuses on differences in the structure and mechanical properties of normal versus transparent dentin. The mineral concentration, as measured by X-ray computed microtomography, was significantly higher in transparent dentin, the elevated concentration being consistent with the closure of the tubule lumens. Crystallite size, as measured by small angle X-ray scattering, was slightly smaller in transparent dentin, although the importance of this finding requires further study. The elastic properties were unchanged by transparency; however, transparent dentin, unlike normal dentin, exhibited almost no yielding before failure. In addition, the fracture toughness was lowered by roughly 20% while the fatigue lifetime was deleteriously affected at high stress levels. These results are discussed in terms of the altered microstructure of transparent dentin.

Keywords: Dentin; Aging; Transparent; Sclerotic; Fracture; Fatigue

1. Introduction

Dentin is the major structural component of the tooth. It is composed of a hydrated organic matrix consisting mostly of type I collagen and an inorganic reinforcing phase of carbonated apatite. Prominent features in the microstructure of dentin are tubules that radiate outward from the pulp to the dentin–enamel junction (DEJ) in coronal dentin, and from the pulp canal to the cementum in the root. In normal human dentin, the tubules are lined with a highly mineralized cuff of peritubular dentin [1,2]. The mineralized collagen fibrils forming the intertubular dentin matrix are arranged in a felt-like structure oriented perpendicular to the tubules.

Although the primary function of dentin is mechanical, it has only been in the last few years that its mechanical properties have begun to be understood in terms of its hierarchical microstructure [3–7]. Recent studies of the elastic constants of dentin have determined that there is a small transverse isotropic symmetry, with the stiffest direction being perpendicular to the tubules [8]. These findings are in agreement with micromechanics arguments that indicate elastic asymmetry would be determined not by the orientation of the

*Corresponding author.
E-mail address: jkinney@itsa.ucsf.edu (J.H. Kinney).

0142-9612/$ - see front matter © 2004 Elsevier Ltd. All rights reserved.
doi:10.1016/j.biomaterials.2004.09.004

tubules, but by the orientation of the collagen fibrils [5]. Additional studies have now shown that the fracture toughness is least in the direction perpendicular to the tubules [7,9], and that so-called uncracked-ligament bridging is a potent toughening mechanism in dentin, particularly in the tubular direction [7,10,11]. Finally, cyclic fatigue also appears to be influenced by dentin microstructure [12,13].

All the studies described above were conducted on healthy dentin, often on unerupted molars. This has been important from the perspective of understanding the fundamental properties of dentin as its microstructure is sufficiently complicated without adding additional uncertainties from mineral variations (e.g., caries) or other age- or disease-related alterations. Nevertheless, many fractures occur in teeth that have been treated, for example restored or endodontically repaired. It is therefore essential to extend these previous studies on healthy dentin to include altered forms of dentin.

One such altered dentin is transparent, or sclerotic, dentin, which forms gradually with aging, beginning at the apical end of the root and often extending into the coronal dentin [14]. Physiologic transparent root dentin, as distinguished from pathologic transparency subjacent to caries, appears to form without trauma or caries attack as a natural part of aging [15]. Transparency occurs when the tubule lumens become filled with mineral, decreasing the amount of light scatter off of the lumens. Specifically, the tubules are filled with a mineral phase; this filling is most likely a passive chemical precipitation [16,17]. It is not clear whether the increased mineralization associated with transparency is entirely a result of the filling of the tubule lumens, or whether there are any additional alterations in the mineralization of the intertubular dentin matrix [18,19].

Because transparency is a common pathology in aged teeth, it is surprising that there have only been a few studies of the relevant mechanical properties. The present work attempts to remedy this by examining the structure and properties of transparent root dentin. We begin by presenting the results of three-dimensional measurements of spatial variations of the mineral concentration in transparent dentin, comparing them with the distributions of mineral in normal dentin. We complete our study of mineralization by quantifying the size of the mineral crystallites in the intertubular dentin matrix. Since the mineralization can affect the elastic behavior [20], we determine the shear and Young's moduli of both normal and transparent root dentin, and present the results here. Finally, we explore fracture, and present the results of the first fracture toughness and cyclic fatigue studies on transparent dentin. The results of these studies are discussed in terms of the altered microstructure of transparent dentin.

2. Materials and methods

2.1. Measurement of the mineral concentration

For measurement of mineral concentration and crystallite size, the teeth were divided into two groups based on transparency. The non-transparent group (normal controls) had an average age of 23.9 (s.d. = 7.0) years, and contained 18 molars and two incisors. Each specimen came from a unique patient. The transparent group had an average age of 80.4 (s.d. = 10.4) years, and contained seven incisors. As before, each specimen was from a unique patient. The teeth were sterilized by gamma radiation and stored in filtered and purified water at 4 °C until imaged. Visual inspection was used to select teeth with transparent root dentin; radiographs and post-imaging sectioning were used to screen teeth for any possible transparency that might have been associated with caries.

For synchrotron radiation computed tomography (SRCT) imaging, the specimens were kept fully hydrated in acrylic, water-filled cells during imaging. The teeth were imaged with X-rays from the 15-period hard X-ray wiggler beamline (10-2) at Stanford Synchrotron Radiation Laboratory (Stanford Linear Accelerator Center, Menlo Park, CA) [21], and at the new X-ray tomography beamline 8.3.2 at the Advanced Light Source (Lawrence Berkeley National Laboratory, Berkeley, CA). Monochromatic (25 keV) X-rays were used. Radiographs were acquired as the specimens were rotated in increments of 0.5° from 0° to 180°. The resulting two-dimensional radiographs were reconstructed into three-dimensional images by Fourier-filtered back projection [22]. The reconstructed three-dimensional images contained a complete spatial mapping of the X-ray attenuation coefficient in each specimen [23,24]. Conversion of the X-ray attenuation coefficient into volume fraction of the mineral phase, V_m, has been described in detail elsewhere [25,26].

Average mineral concentrations at different locations within the tooth were determined by averaging a subvolume selected from the location of interest. Each subvolume contained a minimum of 10,000 volume elements (1 volume element = 7.29×10^{-7} mm^3). Subvolumes were selected to isolate regions in normal or transparent dentin in the cervical root dentin, mid-root dentin, apical root dentin, and in the pre-dentin regions near the wall of the pulp chamber. The data were analyzed for statistical significance using a two-tailed Student t-test [26].

2.2. Determination of the crystallite size in the intertubular dentin matrix

After the tomography scans, four teeth were selected from each of the two groups for small angle X-ray

scattering (SAXS) studies. Sagittal sections, running the length of the teeth, were prepared with an Isomet slow-speed diamond saw. The specimen thickness was 0.25 mm. The SAXS measurements were performed on beam line 1–4 at the Stanford Synchrotron Radiation Laboratory. A description of the experimental apparatus is provided in greater detail elsewhere [27,28].

The synchrotron radiation from a bending magnet was focused in the vertical axis by applying a small curvature to a reflecting mirror in the optical train. The beam was made monochromatic at 0.149 nm by using the reflection from a silicon single crystal. A small bend was applied to this crystal to provide the horizontal focus and increase the flux. Small tungsten apertures were used to collimate the beam size to 0.3 mm vertical by 0.35 mm horizontal at the specimen. The X-ray beam was scanned vertically along the length of the root from the cervical region to the apex in 2 mm steps. The SAXS data from each location were collected on two-dimensional imaging plate detectors (BAS-IIIs) and analyzed by the methods described below. The two-dimensional scattering intensities, $I(x,y)$, were converted to polar coordinates, $I(q,\phi)$, where ϕ was the azimuthal scattering angle, and q was the wave vector given by

$$q = \left(\frac{4\pi}{\lambda}\right)\sin(\theta). \quad (1)$$

Here, λ is the incident X-ray wavelength, and 2θ the scattering angle. Following the procedures described by Guinier and Fournet [29], and applied to bone by Fratzl and co-workers [30–32], the azimuthally averaged scattering intensity could be described as a function of q:

$$I = I_0 T^3 F(qT)(1 + G(q)). \quad (2)$$

where the scattering form factor, $F(q, T)$, is a function of the shape of the crystallites, $G(q)$ is an interference function sensitive to correlations in the crystal positions, and T is a parameter related to the crystallite thickness.

The parameter T, which was associated with the crystallite thickness and had a unit of length, is related to the total surface area, S, and the total volume, V, of the mineral crystals: $T = 4V/S$. T was determined from Porod's observations of scattering at large q:

$$I(q) \to \frac{P}{q^4}. \quad (3)$$

The Porod constant, P, was determined by curve fitting the q^{-4} dependence of the scattering intensity at large q. The data were prepared as Kratky plots and the total scattering yield was calculated. Using the total scattering yield and the Porod constant P, the thickness parameter T could be calculated. The thickness of the crystallites, τ, was estimated from the stereological relationship $\tau = 4T/2$. The thickness data were analyzed for statistical significance using a two-tailed Student t-test.

2.3. Determination of the elastic constants

Resonant ultrasound spectroscopy (RUS) was used to determine the elastic constants of transparent and normal root dentin. Unlike the measurement of sound speed, RUS makes use of Hooke's law and Newton's second law to predict the resonant modes of mechanical vibration of a specimen of known shape [33,34]. From the resonant modes, all of the elastic constants can be uniquely determined from a single measurement if the density of the specimen is known. The application of this technique to normal coronal dentin is described in greater detail elsewhere [8].

Three unerupted human third molars (non-transparent), and three transparent incisors, all from unique patients, were used in this study. Cubes, approximately 2 mm on an edge, were removed from the mid root dentin (Fig. 1a) with a slow-speed diamond saw; tubules were oriented as best as possible at right angles to the top and bottom surfaces of the cube. The specimens were dried, placed between right-angle polishing blocks, and the opposing surfaces were polished flat and parallel. The edges of the specimens were polished to different lengths to avoid a cubic geometry and to better separate the resonant peaks; a typical final dimension was $1.7 \times 1.1 \times 0.8\,\text{mm}^3$. The approximate 2:1 aspect ratio was chosen to increase the sensitivity to detecting anisotropy in low-Q specimens [35].

Three days prior to scanning, the specimens were rehydrated in deionized water and mounted on opposing corners between two transducers in the RUS system (Fig. 1b). The transducers were thin foils of PVDF coated with 300 nm of gold. The resonant frequencies between 0.5 and 1.4 MHz were measured. An approximation of the stiffness tensor was used to generate initial values for the resonant frequencies. The experimental and predicted frequency distributions then were compared, and the residuals were minimized by adjusting the individual terms in the stiffness tensor [33].

2.4. Mechanical testing

Recently extracted transparent human molars ($N = 18$, one tooth per donor) were used for this part of the study (donor age: $\geqslant 65$ years); each tooth was sterilized using gamma radiation after extraction [36]. Sections (~1.5–2.0 mm thick) were prepared vertically through the tooth such that the plane of the fracture was nominally perpendicular to the long axis of the tubules in the root dentin (see Fig. 1a). In actuality, it is almost impossible a priori to align this fracture plane precisely with the tubule axes because, with the exception of the root, the tubules in dentin do not run a straight course from the enamel to the pulp; rather, from the cervical margin through the crown, the tubules have a complex, S-shaped curvature [2]. Consequently, the orientation of

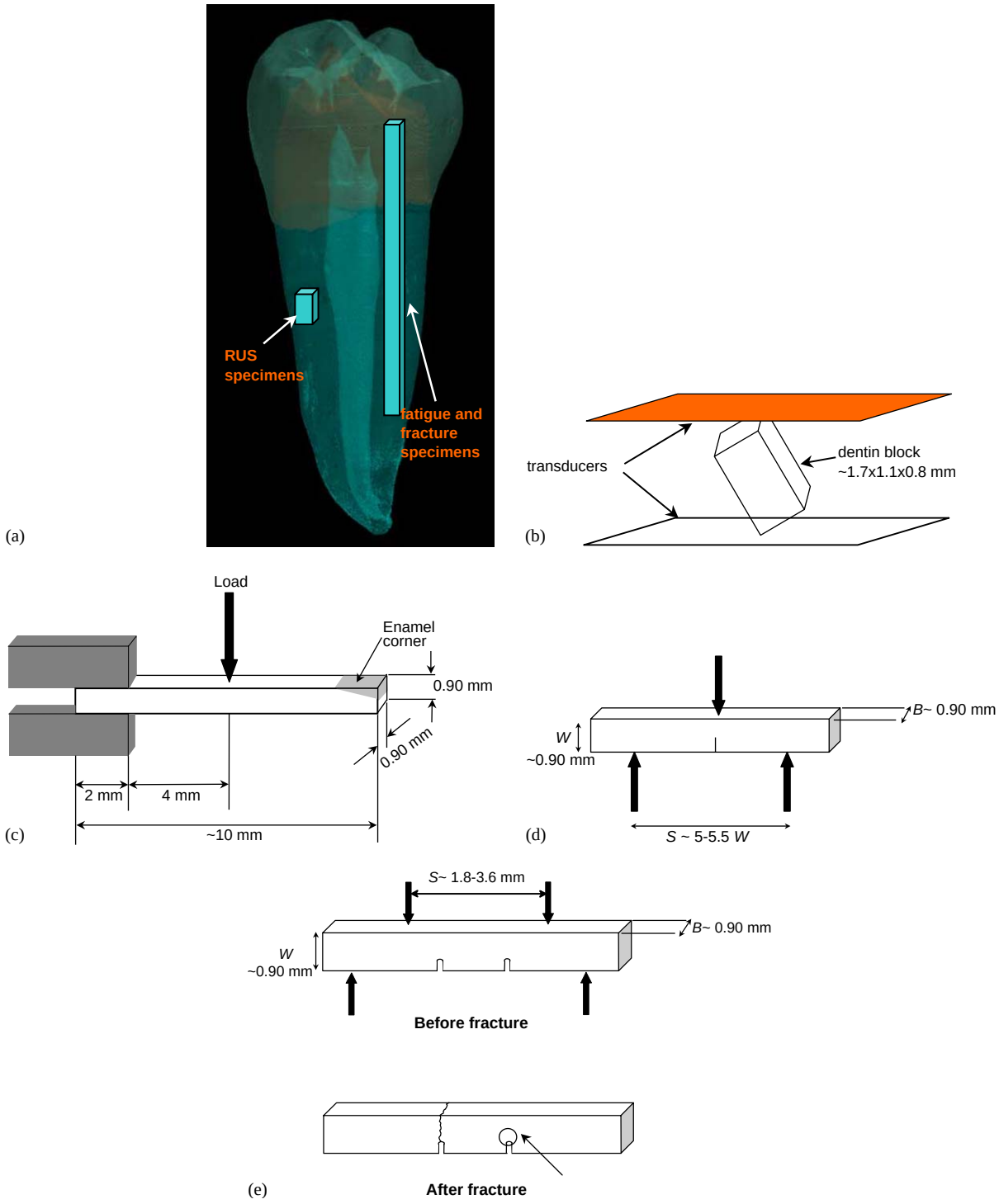

Fig. 1. (a) X-ray tomogram of a premolar showing approximate locations from which specimens were obtained for the RUS and for the fatigue and fracture experiments, and schematic illustrations of (b) the loading geometry used for the RUS experiments, (c) the cantilever-beam geometry used for the deformation/yielding and fatigue stress-life testing, (d) the three-point bending configuration utilized for the fracture toughness measurements, and (e) the double notch four-point bending geometry that was used for investigating the local fracture mechanisms.

the crack plane was determined from examination of the post-test fracture surfaces. In the present study, all toughness and fatigue data were collected on samples where the fracture plane was nominally perpendicular to the average tubule direction.

Eighteen beams, measuring $\sim 0.90 \times 0.90 \times 10.0\,\mathrm{mm}^3$, were prepared from these teeth (one beam per tooth) and wet polishing to a 600 grit finish. The beams were stored in Hanks' Balanced Salt Solution (HBSS) at ambient temperature for no longer than one week until

testing. The results from the testing of transparent dentin were compared with those performed in an identical manner on normal dentin that have been presented elsewhere [7,12,37,38].

First yield (σ_y) and maximum flexural (σ_F) strengths were measured in HBSS by loading the beams ($N = 3$) in cantilever bending (Fig. 1c) on an ELF 3200 series voice-coil mechanical testing machine (EnduraTEC Inc., Minnetonka, MN) using a custom-made Delrin™ loading rig. The applied loads (from the force transducer on the testing frame) and the corresponding load-line displacements (from the displacement transducer on the testing frame) were continuously monitored while the beams were loaded to failure at a constant cross-head displacement rate of 0.01 mm/s. First yield was determined where the load-displacement data deviated from linearity, while the maximum flexural strength was determined from the peak load that the beam sustained prior to catastrophic fracture.

Fracture toughness testing was performed in general accordance with the ASTM Standard E-399 for plane-strain fracture toughness [39]; tests ($N = 3$) were conducted using the three-point bending geometry (Fig. 1d) with a span between the lower two loading points equal to 5–5.5 times the width of the beam ($S \sim 5.5\,W$). A sharp notch was carefully introduced into the top surface of each specimen using a razor blade; typical notch depths were of the order of 50–125 μm, with a root radius, ρ, of ~30–50 μm. Subsequently, in accordance with ASTM E-399, a precrack was grown out of the notch by cycling in fatigue; this was achieved at a load ratio (ratio of minimum to maximum loads) of $R = 0.1$ and loading frequency of 2 Hz, with a final maximum stress-intensity of $K_{max} \sim 0.8\,\mathrm{MPa}\sqrt{\mathrm{m}}$, i.e., well below the estimated fracture toughness of dentin. The final precrack length (notch plus precrack) was of the order of 100–200 μm, with a presumed atomically sharp crack tip.

Fracture toughness testing was conducted with an ELF® 3200 series voice-coil mechanical testing machine (EnduraTEC Inc., Minnetonka, MN). Samples were loaded to failure under displacement control in HBSS at ambient temperature at a cross-head displacement rate of 0.01 mm/s. Applied loads and corresponding displacements, measured again using, respectively, the force and displacement transducers on the testing frame, were monitored throughout the test. The fracture toughness, K_c, was computed from the crack size, a, and load, P_c, at fracture using the expression [39]:

$$K = \left(\frac{P_c S}{B W^{3/2}}\right) f(a/W), \tag{4}$$

where P_c is the applied load, S is the distance between the outer loading pins, a is the crack length, B and W are, respectively, the three-point bend specimen thickness and width, and $f(a/W)$ is dimensionless function of a/W given in Ref. [39]. Further details on the measurement of the fracture toughness in dentin have been presented elsewhere [38]. The K_c results were statistically analyzed using a two-tailed Student t-test. Post-failure observations of the fracture surfaces were made both optically and using a scanning electron microscope (SEM), operating in the secondary electron mode. SEM samples were first coated with a gold–palladium alloy.

To understand the mechanisms associated with how the underlying microstructural features affect deformation and fracture behavior, the double-notch four-point bend geometry [40] was used to generate a stable crack (Fig. 1e). This technique involves loading a beam with two nominally identical notches to failure under four-point bending. Under such loading conditions, both notches experience the same bending moment; thus when one notch fails, the microstructure and local cracking events immediately prior to unstable fracture are effectively "frozen-in" at the unfractured notch.

In the present work, double-notch tests ($N = 3$) were conducted in ambient temperature HBSS, with a span, S, equal to 2–4 times the width, W, of the beam. Rounded notches, of root radius, $\rho \sim 200-300$ μm, and depth, $a \sim 0.3-0.4\,W$, were introduced carefully with a slow-speed saw; care was taken to maintain the specimens in a hydrated state throughout the specimen preparation process. The bend bars were loaded to failure under displacement control using an ELF® 3200 series testing machine at a constant cross head movement rate of 0.01 mm/min. The area around the unfractured notch (indicated in Fig. 1d) was examined using an optical microscope and an SEM.

In addition to fracture testing, the response to repetitive cyclic fatigue loading was also studied using the stress–life approach, akin to that used previously for normal dentin [12,37]. Nine ($N = 9$) beams of transparent dentin were used. S/N fatigue tests were conducted 37 °C HBSS with unnotched cantilever beams cycled on an ELF® 3200 series testing machine using a custom-made Delrin™ loading rig. Testing was performed at a load ratio of $R = 0.1$ at a cyclic frequency of 10 Hz. While this testing frequency is clearly higher than those seen in typical mastication, it was chosen with the purpose of expediting the testing, particularly at long lives ($>10^5$ cycles). The effect of frequency on the fatigue of dentin has been described in our previous work on normal dentin [37].

The dentin beams were cycled to failure under displacement control, with the loads being monitored continuously. Stress–life curves were derived in terms of the initial stress amplitude, σ_a, (given by one half of the difference between the maximum and minimum stresses), based on the nominal bending stress in the beam. The minimum and maximum stress levels employed ranged between, respectively, ~8 and

124 MPa, respectively. The data were analyzed statistically using simple regression.

As in the case of the toughness testing, post-failure observations of the fracture surfaces were made both optically and using a scanning electron microscope. To further observe crack/microstructure interactions, X-ray computed microtomography was performed on two of the fatigue-tested specimens, one normal dentin specimen from a previous study, and one transparent dentin specimen from the current study. The specimens had been cycled for ~120,000 (normal dentin) and ~85,000 (transparent dentin) cycles, and were chosen because they had not fully failed during the fatigue tests, thereby providing the opportunity to examine the comparative role of the microstructure on crack growth.

3. Results

3.1. Mineral concentration and crystallite size

Mineral concentration measurements were made using SRCT, as detailed in Section 2.1. Typical two-dimensional X-ray tomographic reconstructions (the equivalent of thin sections roughly 9 μm thick) for normal (non-transparent) and transparent root dentin are shown in Fig. 2. There was a definite change in the degree of mineralization with transparency, as is evident from the change in contrast in the tomographs. Mean values (and corresponding standard deviations) for the mineral concentrations are given in Table 1 for the four different locations of interest: the cervical third, the middle third, the apical third, and the pre-dentin (near pulp) region. While the mineral content in the transparent dentin near the pulp was significantly higher than the outer transparent dentin (Table 1), in the case of normal dentin, the mineral concentration increased from ~35% in the near-pulp region to ~44% in the remainder of the tooth. Furthermore, there was a statistically significant ($p<0.001$ for all four locations) increase in the level of mineralization with transparency at all four locations where measurements were made. This is particularly evident in the pulpal region where there is a 40% increase in the mineral content in transparent dentin. The mineral concentration in the transparent dentin trended lower on approach to the apex. This gradient was not observed in normal dentin. Thus, the difference in mineral concentration between normal and transparent dentin decreased towards the apex. The transparent dentin always had a greater degree of mineralization.

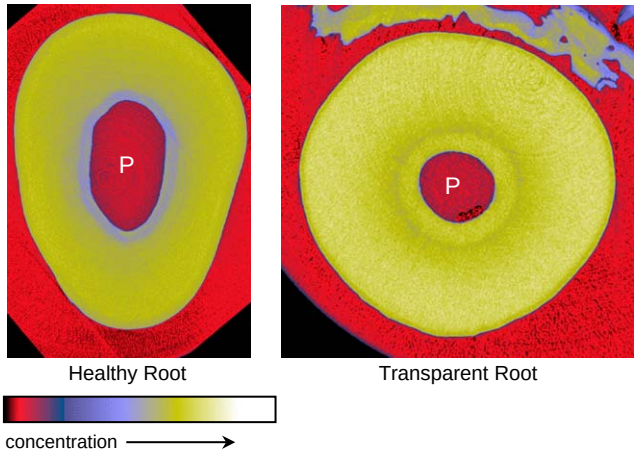

Fig. 2. Typical two-dimensional X-ray tomographic slices for normal (non-transparent) and transparent root dentin. The pulp is indicated with a "P" in both examples. The color scale for mineral concentration is shown at the bottom. The region immediately surrounding the pulp of normal dentin is less mineralized than the interior dentin. In contrast, the dentin near the pulp of the transparent root is hypermineralized to the extent that the mineral concentration is actually greater than the surrounding interior dentin.

Table 1
Mineral concentration (in %) with location in dentin

	Cervical third	Middle third	Apical third	Pulpal region
Normal	44.4±1.6	43.2±1.2	44.0±1.5	35.0±1.8
Transparent	48.4±1.5	46.3±1.2	46.1±0.7	49.0±2.1
	$p<0.001$	$p<0.001$	$p<0.001$	$p<0.001$

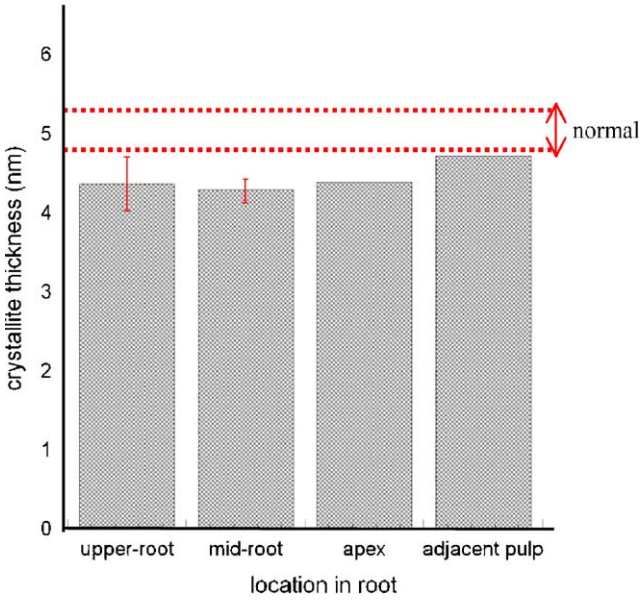

Fig. 3. Mineral crystallite size in transparent dentin, as determined from small angle X-ray scattering experiments. Measurements made at four different locations are shown. The range of values obtained for normal dentin is indicated by the dashed lines. The crystallite size was smaller in the transparent dentin with the exception of the transparent dentin immediately adjacent to the pulp. However, as this latter measurement was obtained from only one tooth, it is not yet possible to determine whether this is statistically significant.

SAXS studies determined a mean crystallite size from sagittal sections of normal and transparent dentin; corresponding results are shown in Fig. 3. The range

of crystallite size for normal dentin is spanned by the two solid lines, while the size measured in transparent dentin is shown as a mean and standard deviation. At all locations, the mean size of the crystallites in transparent dentin was lower ($p<0.01$); however it is not yet clear if this is a physical result or perhaps due to differences in the scattering from the filled tubules lumens that might affect the measurement of the Porod constant (Eq. (4)) in transparent dentin (an exception is the SAXS measurement obtained near the pulp of a single specimen, which appeared to have normal size). Although more detailed SAXS experiments are planned, it can be stated that the crystallite size is definitely not larger in transparent dentin, as would be the case if additional mineral were to have been accreted onto the existing surfaces during the transparency process.

3.2. Elastic constants of normal and transparent root dentin

Fig. 4 shows data for elastic moduli obtained by resonant ultrasound spectroscopy. Isotropic shear moduli of ~10.1 GPa (s.d. = 0.5) in transparent dentin, and 10.3 GPa (s.d. = 0.1) in normal dentin were recorded. Isotropic Young's moduli of ~26.0 GPa (s.d. = 1.4) and 26.7 GPa (s.d. = 0.7) were also obtained for transparent and normal dentin, respectively. The differences between normal and transparent dentin were not significant. The magnitudes of the elastic constants are consistent with previous RUS and indentation studies of dentin [6,8].

3.3. Deformation behavior

Typical load-displacement data for transparent dentin is shown in Fig. 5, together with similar results for normal dentin from a previous study [7]. Macroscopically, there was clear evidence of "yielding" and post-yield inelastic deformation in normal dentin, substantiated by the deviation from linearity in the load-displacement data, akin to that commonly observed in bone (e.g., [41]). Surprisingly, corresponding evidence of yielding was effectively non-existent in the transparent dentin. Consequently, the measured first yield (σ_y) and maximum flexural (σ_F) strengths were identical in the transparent dentin, i.e., $\sigma_y \sim \sigma_F = 170.6$ (s.d. = 7.86) MPa, as compared to $\sigma_y \sim 75$ MPa and $\sigma_F \sim 160$ MPa, respectively, for normal dentin [38]; possible mechanisms for this difference in behavior are discussed below.

3.4. Fracture toughness behavior

A mean fracture toughness, K_c, of 1.46 (s.d. = 0.11) MPa$\sqrt{m}$ was obtained for transparent dentin using three-point bend testing (Fig. 6). This toughness was some 20% lower than that measured using similar procedures for normal dentin (1.79 ± 0.06 MPa$\sqrt{m}$ [38]. The differences between the two were found to be statistically significant using a two-tailed Student t-test

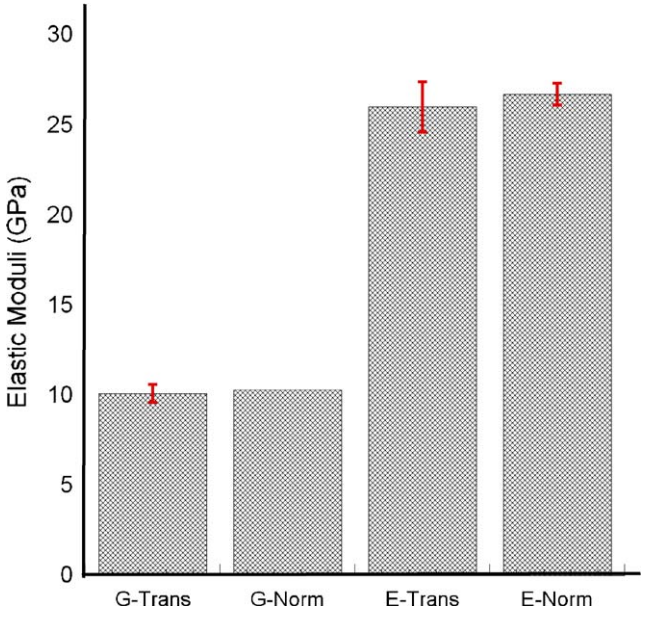

Fig. 4. Elastic moduli for dry dentin obtained using resonant ultrasound spectroscopy for normal ("Norm") and transparent ("Trans") dentin. The shear modulus, G, and the Young's modulus, E, were obtained from a single measurement. The resonant frequencies were consistent with an isotropic symmetry model, in agreement with earlier findings on dry coronal dentin [8].

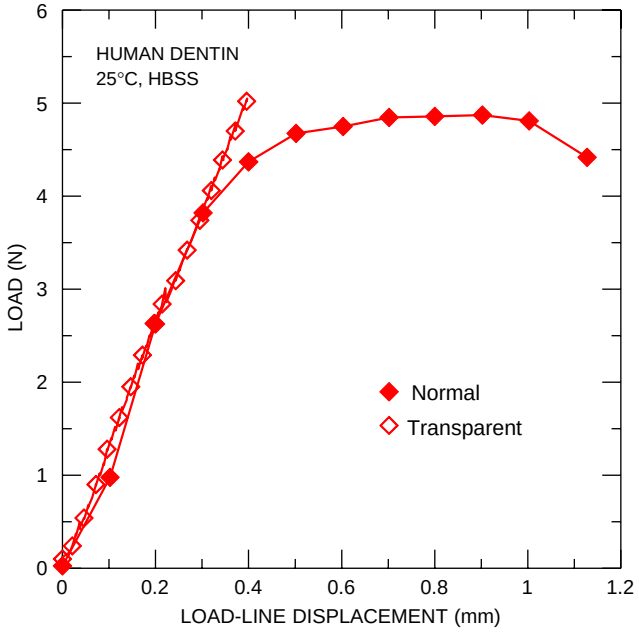

Fig. 5. Typical load-displacement data for normal and transparent dentin. Note the extensive post-yield behavior in normal dentin that is essentially absent in the transparent case.

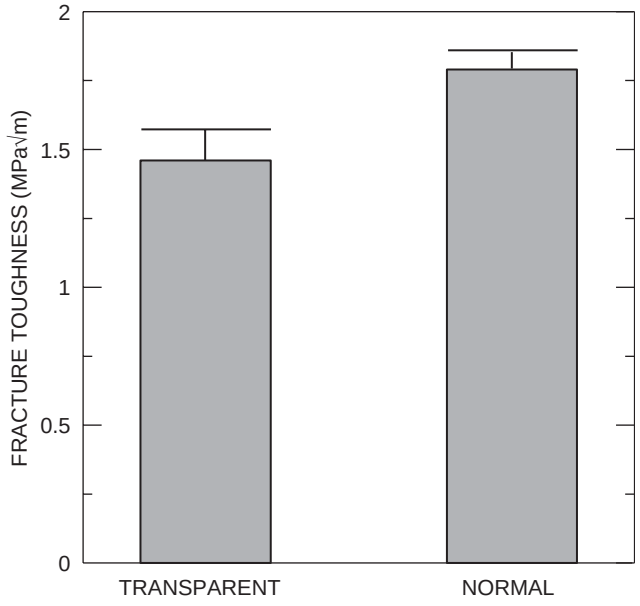

Fig. 6. The mean values of the measured fracture toughness, K_c, for normal and transparent dentin. The half error bars represent one standard deviation.

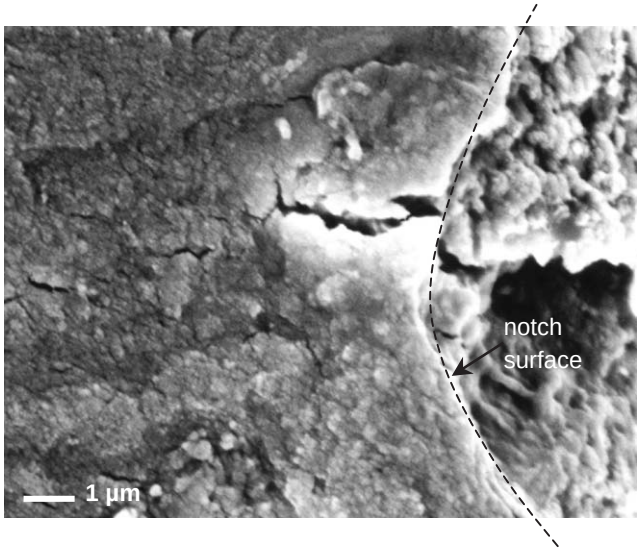

Fig. 7. Scanning electron micrograph showing a crack emanating from the unfractured notch in a double-notched bending experiment on transparent dentin.

$(t(4) = 4.45, p < 0.05)$, implying that age-induced transparency lowers the fracture resistance of dentin.

Fig. 7 shows a typical micrograph of the results from the double-notched four-point bend tests. Though crack initiation appears to occur from the notch itself, the absence of substantial inelastic deformation in transparent dentin implies that, in contrast to normal dentin [42], the distinction between stress- and strain-controlled fractures cannot be unequivocally achieved by the double notch experiment. Furthermore, attempts to obtain more substantial crack growth in order to observe the crack-microstructure interaction failed, presumably due to the more "brittle" nature of transparent dentin.

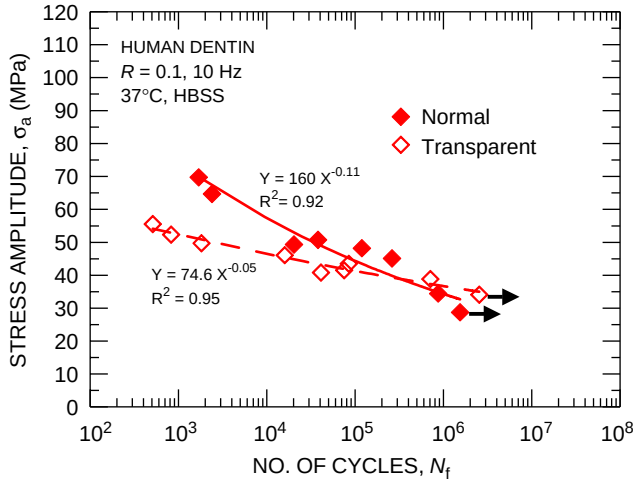

Fig. 8. Stress–life S/N fatigue data for normal and transparent dentin. The power law fits (with corresponding coefficients of determination, R^2) are also shown. Note the difference in fatigue behavior at high stress levels, where the fatigue life of transparent dentin is significantly lower. Arrows indicate "run-out" specimens that did not fail within the designated number of cycles.

3.5. Stress–life fatigue behavior

Stress–life data, obtained for transparent dentin at a cyclic frequency of 10 Hz with $R = 0.1$, are shown in Fig. 8 in the form of the number of fatigue cycles to failure, N_f, as a function of the applied stress amplitude, σ_a; these results are compared with corresponding data for normal dentin from earlier work [12]. Each reported lifetime is from a single specimen. Cyclic fatigue data spanning about five decades in life, from $\sim 10^2$ to 10^7 cycles, were obtained for stresses between ~8 and 124 MPa, representing values of ~5% and 73% of the maximum flexural strength of transparent dentin. It is evident that, like normal dentin, transparent dentin shows "metal-like" fatigue behavior in that fatigue lifetimes increase with decreasing stress amplitudes until an apparent plateau, resembling a fatigue limit, is reached at $\sim 10^6$ cycles.

From the mathematical fits shown in Fig. 8, values for this apparent fatigue limit for high-cycle fatigue were practically identical for normal and transparent dentin, i.e., respectively, 34.3 and 36.7 MPa. Such fatigue limits represented values of approximately 20% of the measured tensile strength, i.e., comparable with most metallic materials where the fatigue limit at this load ratio is typically 25–30% of the tensile strength [43]. However, at higher stress levels in the so-called low-cycle fatigue regime, specifically for stress amplitudes

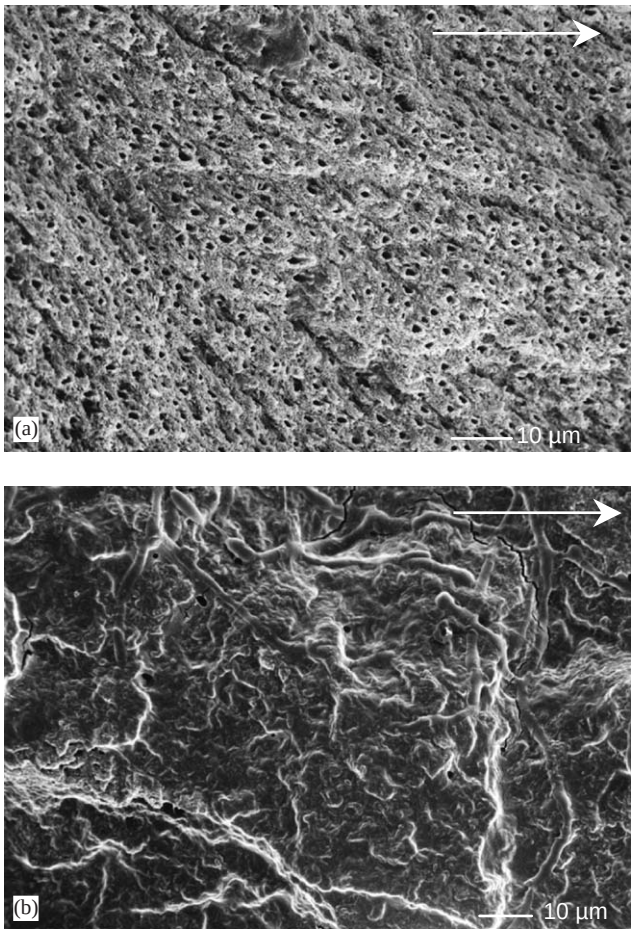

Fig. 9. Scanning electron micrographs showing typical fatigue fracture surfaces for (a) normal dentin, and (b) transparent dentin. Note that a majority of the tubules in the imaged area are filled in transparent dentin, leading to the rather "flat" appearance of the fracture surface. The white arrows indicate the nominal direction of crack growth.

between 45 and 70 MPa, transparent dentin appears to have much poorer resistance to fatigue, in terms of shorter fatigue lifetimes at a given stress level. Such differences are diminished at lower stress levels in the high-cycle regime, and in fact, there appears to be some reversal in the observed trends, although there are insufficient data to arrive at definitive conclusions.

Fractography of the fracture surfaces (Fig. 9) revealed a rather "flat" fracture surface for transparent dentin in areas where the tubule lumens had been filled, in contrast to normal dentin where the tubules are clearly visible intersecting the surface.

3.6. X-ray computed tomography of the crack path

An understanding of the differences in fatigue and fracture behavior between normal and transparent dentin were obtained from SRCT imaging of partially failed fatigue specimens. Fig. 10 shows a three-dimensional reconstruction of two such cracked specimens,

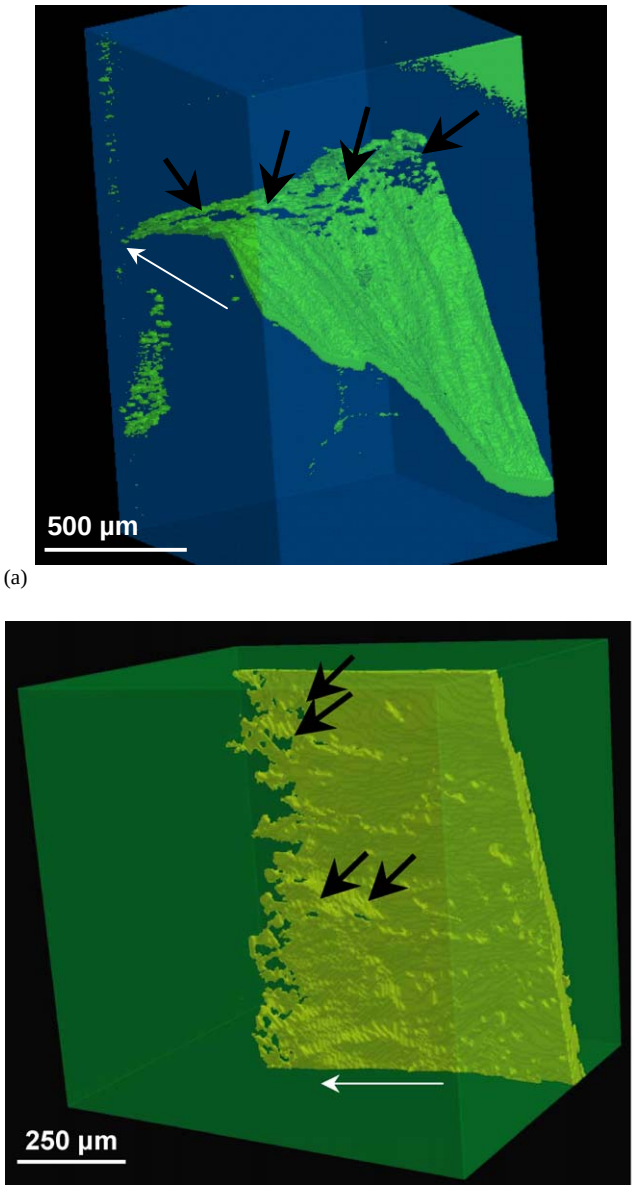

Fig. 10. Three-dimensional X-ray tomographic reconstructions of fatigue cracks in (a) normal dentin, and (b) transparent dentin. Note the clear evidence of uncracked ligaments (indicated by black arrows) in the wake of the crack in normal dentin. The white arrow in each case indicates the direction of nominal fatigue-crack growth.

one each of normal and transparent dentin. In the case of normal dentin, there is definitive visual evidence of so-called "uncracked ligaments"—bridges of unbroken dentin that span the crack— in the crack wake (Fig. 10a). Such bridging has been previously identified as a potent mechanism of toughening in dentin [10,11]. By contrast, in transparent dentin, there is almost no bridging (Fig. 10b), except very close to the crack tip. What few bridges do exist in transparent dentin were small in cross section, and probably contribute little to the fracture toughness.

4. Discussion

One conclusion from this work is that the mineral concentration is significantly higher in transparent root dentin than in normal dentin. Of importance is whether this increase in mineral concentration is due only to the closure of the tubule lumens, or whether there is an additional accretion of mineral into the intertubular dentin matrix, as had been suggested in the past [19]. It is likely that the majority, if not all, of the increased mineral concentration is due to the closure of the tubule lumens. In a microradiographic survey, Weber [44] was unable to detect any difference in mineral concentration of the intertubular dentin between normal and age-related dentins, and attributed all of the increase in the average mineral content to the increased accumulation of mineral salts in the tubule lumens. A similar finding was reported by Vasiliadis et al. [17]. Indeed, when we account for tubule density [45], our tomography results are also consistent with this interpretation. In addition, the observed trend in our data towards a decreasing difference in mineral concentration between normal and transparent dentin with approach to the root apex is also consistent with the observed decrease in the tubule density from the cervical dentin towards the apex [45,46].

Crystallite size was slightly lower in transparent dentin. As mentioned previously, the measurement of the Porod constant might have been affected by a noticeable fiber ("bow-tie") pattern in the scattering from the transparent dentin. We think this is unlikely, however, since only scattering perpendicular to the contributions from the fiber texture was analyzed. Therefore, assuming that the mineral crystallites in transparent dentin are indeed smaller, we suggest two possible explanations why the SAXS results might be true. First, a smaller mean size might result from the dissolution of mineral from the intertubular matrix into the tubule lumens. On the other hand, a reduction of the mean crystallite size could also be caused by precipitation of new, but smaller, crystallites within the matrix. Whatever mechanism causes the deposition within the lumens might also lead to nucleation within the intertubular dentin matrix. A passive precipitation within the intertubular dentin matrix need not lead to any changes in the elastic properties [47]. Whether there is dissolution or passive precipitation, the alterations would have to be small, since prior radiographic studies were unable to detect changes in the net mineral concentration within the intertubular matrix [44]. Clearly, more study is warranted on this issue.

We observed significant hypermineralization of the pulpal region; absence of a normal, pre-dentin layer was also noted by Vasiliadis et al. [15,17]. It is likely that the high density of filled tubule lumens in dentin near the pulpal boundary can account for much of this hypermineralization, although additional accretion of mineral into the intertubular matrix cannot be ruled out. Further study of this region with microradioagraphy and nanoindentation is needed.

If the major alteration in transparent dentin is simply the accretion of mineral in the tubule lumens, then we need to address how this might change the elastic properties. We have previously determined that tubules should have only a minor affect on the elastic properties of dentin [5]. Based on this argument, we would therefore expect the elastic constants of transparent and normal dentin to be the same within measurement sensitivity as long as the intertubular dentin matrix was unaltered. Because earlier work by Balooch et al. [48] indicated that the hardness and modulus of the intertubular transparent dentin was the same as that of normal dentin, it therefore came as no surprise that the RUS measurements were unable to detect a statistical difference in either the Young's modulus or the shear modulus, supporting the hypothesis that the intertubular dentin matrix is substantially unaltered.

If the elastic constants are unaltered by transparency, then we might expect that fracture properties would also be unchanged. Our study shows this is not the case, as fracture toughness was lower by roughly 20%, or 0.33 MPa $m^{1/2}$. This has a clinically significant impact; the critical flaw size, i.e., the largest crack that can be tolerated without failure, calculated from such toughness values decreases by roughly a third at a nominal mastication stress of 20 MPa [49] (Fig. 11). Therefore, the susceptibility of the root to fracture is increased by

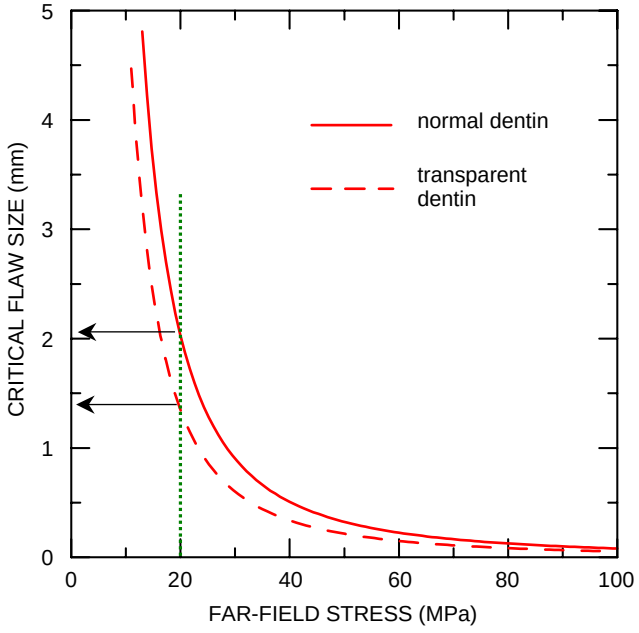

Fig. 11. Calculated critical flaw sizes with far-field (applied) stresses for both normal and transparent dentin. Note the roughly 33% reduction in such predictions with transparency at a physiologically relevant stress level for normal mastication [49] of 20 MPa.

imperfections that might be introduced during endodontic treatments or restoration of caries lesions.

Why should the fracture toughness be lower in transparent dentin? One possibility is that transparent dentin, because the tubules are occluded, is less hydrated than normal dentin. This could reduce crack-tip blunting, which has been observed in hydrated dentin, thereby decreasing the fracture toughness. We consider this to be unlikely, however. The elastic constants are known to be sensitive to the level of hydration [8]. The absence of any discernable difference in the flexural modulus of normal and transparent dentin is a strong indication that the hydration levels were the same in the two dentins. Furthermore, the high-cycle fatigue properties, believed to reflect the alternate blunting and sharpening of the crack tip, are the same in the two types of dentin. If hydration was an issue, we would have expected differences in the high-cycle fatigue data, and not, as observed, in the low-cycle fatigue data, which is believed to be mediated by crack bridging.

We offer the following hypothesis, which is based upon earlier studies [7,10] that have shown the importance of uncracked-ligament bridging in resisting crack propagation. Uncracked ligaments are tracts of unbroken dentin (roughly 50–250 μm thick) that span the crack and reduce the driving stress at the crack tip (Fig. 10). During dynamic studies, we have observed microcracks nucleating at the tubules ahead of the advancing crack tip [10,11]. We hypothesize that these microcracks, during the process of linking back to the primary crack, spawn uncracked ligaments that persist for up to half a millimeter or more behind the crack tip. We have estimated that the uncracked ligaments should contribute roughly 1 MPa $m^{1/2}$ to the fracture toughness [11], as they act to sustain part of the applied load that would otherwise contribute to crack propagation.

A close examination of the tomography images in Fig. 10 reveals little to no bridging in the wake of the crack in transparent dentin, indicating that uncracked ligaments might not be forming in transparent dentin. Only at the very tip of the crack is there any evidence of ligament formation, and these are small, on the order of 20 microns or thinner. This is in stark contrast to the tomographic images in normal dentin, where large (~250 μm) ligaments can be seen in the crack wake upwards of 0.5 mm from the crack tip.

We believe that filling the tubules acts to reduce the stress concentration associated with the peritubular cuff, thereby lowering the tendency for microcrack nucleation there. In the absence of significant microcrack nucleation well ahead of the main crack tip, uncracked ligaments are less likely to form, which in turn lowers the fracture toughness of the dentin. This model is schematically represented in Fig. 12.

The measured reduction in fracture toughness, however, was only a third of what would be predicted if all

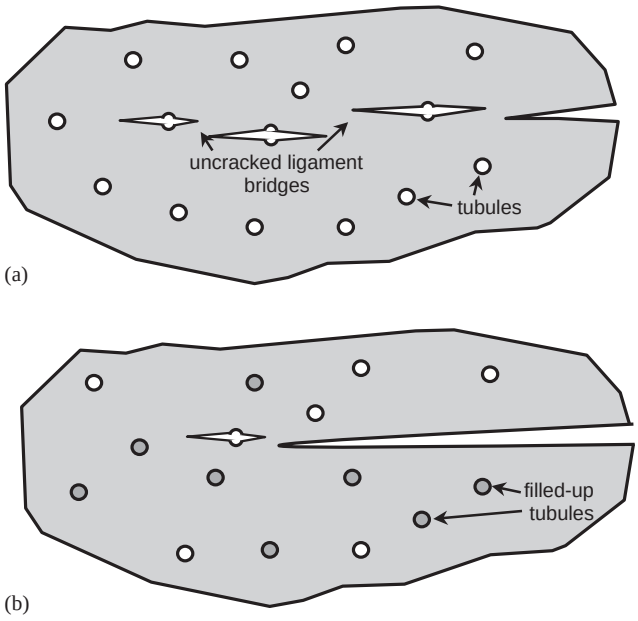

Fig. 12. Schematic illustrations of the differences in proposed fracture mechanisms in (a) normal dentin, and (b) transparent dentin. In normal dentin, microcrack formation at peritubular cuffs ahead of the crack tip leads to the formation of uncracked ligaments due to imperfect link-ups between the microcracks and the main crack tip. With transparent dentin, mineral accretion seals up some of the tubules, leading to fewer stress concentration points ahead of the crack tip, and hence, fewer (if any) uncracked-ligament bridges are formed. The absence of such bridges, which normally increase the toughness by sustaining part of the applied loads that would otherwise be used for crack extension, results in the diminished fracture toughness of transparent dentin.

ligaments were absent. This can be explained by the observation that in physiologic transparent root dentin only 20–50% of the tubules appear to be filled [44]. Thus, some number of microcracks could still form ahead of the crack tip and lead to some additional toughening by our proposed mechanism.

The major finding of this work was that fracture was significantly affected by the presence of transparency. Compared to normal dentin, transparent dentin has a lower toughness and much reduced "plasticity", i.e., it displays nominally ideally brittle behavior with first yield and failure stresses being identical. These findings are clinically relevant, since transparency is a natural consequence of age. Indeed, we suggest that root transparency might be the underlying cause of the perceived fragility of endodontically treated teeth. Therefore, restorative procedures in aged individuals might require modification to accommodate the reduced fracture toughness of the dentin tissue.

Early belief that transparency required a vital pulp (e.g., [50]) has been largely discounted [51]. It now appears that endodontically restored teeth have the same or greater rate of transparent dentin formation as vital teeth [51]. It would be of great benefit, therefore, if clinical studies of tooth fracture would report

the presence and extent of transparency in the fractured teeth.

Irrespective of the immediate clinical relevance to root fracture, our findings provide an important insight into the effects of aging on mineralized tissue. Because dentin does not undergo remodeling, one can argue that dentin is the oldest collagen-based mineralized tissue in the body. Therefore, the effects of aging on the mineralized collagen scaffolding should be most apparent in dentin. Clearly, transparent teeth are brittle in comparison with healthy dentin. We believe that this increased brittleness of transparent dentin is a direct result of a microstructural alteration, namely the filling of the tubule lumens.

There is no convincing evidence, based upon these studies, which would suggest the mineralized collagen scaffold is significantly altered, and therefore is a cause of the increased brittleness. Therefore, it is natural to offer the following hypothesis: the observed increase in brittle behavior of mineralized tissues with age is caused by age-related microstructural alterations of the tissue that do not involve deterioration of the mineralized collagen scaffold. In teeth, the microstructural alteration would be filling of the tubule lumens. In bone, the microstructural alterations might be manifold, including increased density of weak interfaces (e.g., cement lines), or loss of tissue due to bone turnover. The evidence that we have offered to support this hypothesis is suggestive but not conclusive. For this, it will be necessary to repeat the above studies on aged dentin that is not transparent; furthermore, larger sample sizes are needed to address inter-donor variability and to confirm our observations. Such additional studies are planned.

5. Conclusions

Based on an investigation of the mineral content, crystallite size and mechanical properties of transparent dentin, the following conclusions can be made:

1. Synchrotron radiation computed tomography imaging showed that there was an increase in the level of mineralization with transparency. Small angle X-ray scattering studies further revealed that the crystallite size in transparent dentin was smaller than in normal dentin.
2. Isotropic shear ($\sim$10 GPa) and Young's ($\sim$26.5 GPa) moduli were measured using resonant ultrasound spectroscopy; differences between normal and transparent dentin were not significant.
3. In contrast to normal dentin, transparent dentin did not show much "yielding", as evidenced by the relative absence of non-linearity in the load-displacement deformation behavior. Since, the major microstructural change accompanying transparency is the accretion of mineral in the tubule lumens, this difference in behavior suggests that yielding in dentin is the result of microcracking at the tubule sites.
4. A mean fracture toughness 1.5 MPa$\sqrt{\text{m}}$ was obtained for transparent dentin using three-point bend testing, some 20% lower than that measured for normal dentin.
5. Similar to normal dentin, transparent dentin showed "metal-like" cyclic fatigue behavior in that fatigue lifetimes increased with decreasing stress amplitudes until an apparent plateau, resembling a fatigue limit, was reached. The fatigue limit in transparent dentin was $\sim$36.7 MPa at $\sim 10^6$ cycles. However, at higher stress levels in the so-called low-cycle fatigue regime, specifically for stress amplitudes between 45 and 70 MPa, transparent dentin appears to have much poorer resistance to fatigue, in terms of shorter fatigue lifetimes at a given stress level. Such differences are diminished at lower stress levels in the high-cycle regime.
6. Synchrotron imaging of partially failed fatigue specimens revealed that there was almost no crack bridging in transparent dentin, except very close to the crack tip, in contrast to normal dentin, where extensive bridging ligaments were observed. The absence of such bridges, which normally increase the toughness by sustaining part of the applied loads that would otherwise be used for crack extension, results in the diminished fracture toughness of transparent dentin. This is believed to be the result of tubules getting filled with mineral in transparent dentin, leaving fewer sites for ligament formation ahead of a crack tip.

Acknowledgements

This work was supported by the National Institutes of Health under Grant No. P01DE09859 (for RKN and JHK) and by the Director, Office of Science, Office of Basic Energy Science, Division of Materials Sciences and Engineering, Department of Energy under No. DE-AC03-76SF00098 (for ROR) and DE-AC03-76SF00515 (JAP). We also acknowledge the support of the Small-Angle Scattering Facility (BL 1-4) at the Stanford Synchrotron Radiation Laboratory (SSRL), supported by Department of Energy contract No. DE-AC03-76SF00515, and the dedicated tomography beamline 8.3.2 at the Advanced Light Source (ALS), supported by the Department of Energy (BES) under Contract No. DE-AC03-76SF00098. Finally, we also wish to thank Profs. S. J. and G.W. Marshall, and A. P. Tomsia for their support, and Ms. G. Nonomura for specimen preparation.

References

[1] Pashley DH. Dentin: a dynamic substrate—a review. Scanning Microsc 1989;3:161–74 discussion 174–76.

[2] Ten Cate AR. Oral histology-development, structure and function. St. Louis, MO: Mosby; 1994. p. 173.

[3] Angker L, Swain MV, Kilpatrick N. Micro-mechanical characterisation of the properties of primary tooth dentine. J Dent 2003;31:261–7.

[4] Kahler B, Swain MV, Moule A. Fracture-toughening mechanisms responsible for differences in work to fracture of hydrated and dehydrated dentine. J Biomech 2003;36:229–37.

[5] Kinney JH, Balooch M, Marshall GW, Marshall SJ. A micromechanics model of the elastic properties of human dentine. Arch Oral Biol 1999;44:813–22.

[6] Kinney JH, Marshall SJ, Marshall GW. The mechanical properties of human dentin: a critical review and re-evaluation of the dental literature. Crit Rev Oral Biol Med 2003;14:13–29.

[7] Nalla RK, Kinney JH, Ritchie RO. Effect of orientation on the in vitro fracture toughness of dentin: the role of toughening mechanisms. Biomaterials 2003;24:3955–68.

[8] Kinney JH, Gladden JR, Marshall GW, Marshall SJ, So JH, Maynard JD. Resonant ultrasound spectroscopy measurements of the elastic constants of human dentin. J Biomech 2004;37:437–41.

[9] Iwamoto B, Ruse ND. Fracture toughness of human dentin. J Biomed Mater Res 2003;66A:507–12.

[10] Kruzic JJ, Nalla RK, Kinney JH, Ritchie RO. Crack blunting, crack bridging and resistance-curve fracture mechanics in dentin: effect of hydration. Biomaterials 2003;24:5209–21.

[11] Nalla RK, Kruzic JJ, Ritchie RO. On the origin of the toughness of mineralized tissue: microcracking or crack bridging? Bone 2004;34:790–8.

[12] Nalla RK, Imbeni V, Kinney JH, Staninec M, Marshall SJ, Ritchie RO. In vitro fatigue behavior of human dentin with implications for life prediction. J Biomed Mater Res 2003;66A:10–20.

[13] Arola DD, Rouland JA. The effects of tubule orientation on fatigue crack growth in dentin. J Biomed Mater Res 2003;67A:78–86.

[14] Micheletti Cremasco M. Dental histology: study of aging processes in root dentine. Boll Soc Ital Biol Sper 1998;74:19–28.

[15] Vasiliadis L, Darling AI, Levers BG. The amount and distribution of sclerotic human root dentine. Arch Oral Biol 1983;28:645–9.

[16] Natusch I, Pilz ME, Klimm W, Buchmann G. Transparent dentinal sclerosis and its clinical significance. Zahn Mund Kieferheilkd Zentralbl 1989;77:3–7.

[17] Vasiliadis L, Darling AI, Levers BG. The histology of sclerotic human root dentine. Arch Oral Biol 1983;28:693–700.

[18] Giachetti L, Ercolani E, Bambi C, Landi D. Sclerotic dentin: aetiopathogenetic hypotheses. Minerva Stomatol 2002;51:285–92.

[19] van Huysen G. The microstructure of normal and sclerosed dentine. J Prosthet Dent 1960;10:976.

[20] Angker L, Nockolds C, Swain MV, Kilpatrick N. Correlating the mechanical properties to the mineral content of carious dentine-a comparative study using an ultra-micro indentation system (UMIS). Arch Oral Biol 2004;49:369–78.

[21] Karpenko V, Kinney JH, Kulkarni S, Neufeld K, Poppe C, Tirsell KG, Wong J, Cerino J, Troxel T, Yang J. Beamline-10—a multipole wiggler beamline at SSRL. Rev Sci Instrum 1989;60:1451–6.

[22] Kinney JH, Nichols MC. X-ray tomographic microscopy (xtm) using synchrotron radiation. Annual Rev Mater Sci 1992;22:121–52.

[23] Kinney JH, Marshall GW, Marshall SJ. Three-dimensional mapping of mineral densities in carious dentin: theory and method. Scanning Microsc 1994;8:197–204 discussion 204–05.

[24] Kinney JH, Haupt DL, Nichols MC, Breunig TM, Marshall GW, Marshall SJ. The X-ray tomographic microscope—3-dimensional perspectives of evolving microstructures. Nucl Instrum Methods A 1994;374:480–6.

[25] Kinney JH, Haupt DL, Balooch M, Ladd AJC, Ryaby JT, Lane NE. Three-dimensional morphometry of the L6 vertebra in the ovariectomized rat model of osteoporosis: biomechanical implications. J Bone Miner Res 2000;15:1981–91.

[26] Nuzzo S, Peyrin F, Cloetens P, Baruchel J, Boivin G. Quantification of the degree of mineralization of bone in three-dimensions using synchrotron radiation microtomography. Medical Physics 2002;29:2672–81.

[27] Kinney JH, Pople JA, Marshall GW, Marshall SJ. Collagen orientation and crystallite size in human dentin: a small angle X-ray scattering study. Calcif Tissue Int 2001;69:31–7.

[28] Kinney JH, Popel JA, Driessen CKH, Breunig TM, Marshall GW, Marshall SJ. Intrafibrillar mineral may be absent in dentinogenesis imperfecta type-II (DI-II). Journal of Dental Research 2001;80:1555–9.

[29] Guinier A, Fournet G. Small-angle scattering of X-rays. New York: Wiley; 1955. p. 267.

[30] Rinnerthaler S, Roschger P, Jakob HF, Nader A, Klaushofer K, Fratzl P. Scanning small angle X-ray scattering analysis of human bone sections. Calcif Tissue Int 1999;64:422–9.

[31] Roschger P, Grabner BM, Rinnerthaler S, Tesch W, Kneissel M, Berzlanovich A, Klaushofer K, Fratzl P. Structural development of the mineralized tissue in the human L4 vertebral body. J Struct Biol 2001;136:126–36.

[32] Paris O, Zizak I, Lichtenegger H, Roschger P, Klaushofer K, Fratzl P. Analysis of the hierarchical structure of biological tissues by scanning X-ray scattering using a micro-beam. Cell Mol Biol (Noisy-le-grand) 2000;46:993–1004.

[33] Migliori A, Sarrao JL, Visscher WM, Bell TM, Lei M, Fisk Z, Leisure RG. Resonant ultrasound spectroscopic techniques for measurement of the elastic moduli of solids. Physica B 1993;183:1–24.

[34] Maynard JD. Resonant ultrasound spectroscopy. Phys Today 1996;49:26–31.

[35] Ulrich TJ, McCall KR, Guyer RA. Determination of elastic moduli of rock samples using resonant ultrasound spectroscopy. J Acoust Soc Am 2002;111:1667–74.

[36] White JM, Goodis HE, Marshall SJ, Marshall GW. Sterilization of teeth by gamma radiation. J Dent Res 1994;75:1560–7.

[37] Nalla RK, Kinney JH, Marshall SJ, Ritchie RO. On the in vitro fatigue behavior of human dentin: effect of mean stress. J Dent Res 2004;83:211–5.

[38] Imbeni V, Nalla RK, Bosi C, Kinney JH, Ritchie RO. In vitro fracture toughness of human dentin. J Biomed Mater Res 2003;66A:1–9.

[39] ASTM E399-90 (Reapproved 1997). Annual Book of ASTM Standards, vol. 03.01: Metals—mechanical testing; elevated and low-temperature tests; metallography. West Conshohocken, ASTM; Pennsylvania, USA: 2002.

[40] Nalla RK, Kinney JH, Ritchie RO. Mechanistic fracture criteria for the failure of human cortical bone. Nature Mater 2003;2:164–8.

[41] Wang X, Shen X, Li X, Agrawal CM. Age-related changes in the collagen network and toughness of bone. Bone 2002;31:1–7.

[42] Nalla RK, Kinney JH, Ritchie RO. On the fracture of human dentin: is it stress- or strain-controlled? J Biomed Mater Res 2003;67A:484–95.

[43] Suresh S. Fatigue of materials, 2nd ed. Cambridge: Cambridge University Press; 1998.

[44] Weber DF. Human dentine sclerosis: a microradiographic survey. Arch Oral Biol 1974;19:163–9.
[45] Whittaker DK, Kneale MJ. The dentine-predentin interface in human teeth. Brit Dent J 1979;146:43–6.
[46] Carrigan PJ, Morse DR, Furst ML, Sinai IH. A scanning electron microscopic evaluation of human dentinal tubules according to age and location. J Endodont 1984;10:359–63.
[47] Kinney JH, Habelitz S, Marshall SJ, Marshall GW. The importance of intrafibrillar mineralization of collagen on the mechanical properties of dentin. J Dent Res 2003;82:957–61.
[48] Balooch M, Demos SG, Kinney JH, Marshall GW, Balooch G, Marshall SJ. Local mechanical and optical properties of normal and transparent root dentin. J Mater Sci Mater Med 2001;12:507–14.
[49] Anderson DJ. Measurement of stress in mastication I. J Dent Res 1956;35:664–70.
[50] Bang G, Ramm E. Determination of age in humans from root dentine transparency. Acta Odonto. Scand 1970;28:3–35.
[51] Thomas GJ, Whittaker DK, Embery G. A comparative study of translucent apical dentine in vital and non-vital human teeth. Arch Oral Biol 1994;39:29–34.